Dose limited reliability of quantitative annular dark field scanning transmission electron microscopy for nano-particle atom-counting

Reference:

de Backer Annick, Martinez Gerardo, MacArthur K.E., Jones L., Béché Armand, Nellist P.D., Van Aert Sandra.- Dose limited reliability of quantitative annular dark field scanning transmission electron microscopy for nano-particle atom-counting Ultramicroscopy - ISSN 0304-3991 - 151(2015), p. 56-61

DOI: http://dx.doi.org/doi:10.1016/j.ultramic.2014.11.028

Dose limited reliability of quantitative annular dark field scanning transmission electron microscopy for nano-particle atom-counting

A. De Backer[a], G.T. Martinez[a], K.E. MacArthur[b], L. Jones[b], A. Béché[a], P.D. Nellist[b], S. Van Aert[a,1,*]

[a] *Electron Microscopy for Materials Science (EMAT), University of Antwerp, Groenenborgerlaan 171, B-2020 Antwerp, Belgium*
[b] *Department of Materials, University of Oxford, 16 Parks Road, Oxford, OX1 3PH, UK*

Abstract

Quantitative annular dark field scanning transmission electron microscopy (ADF STEM) has become a powerful technique to characterise nano-particles on an atomic scale. Because of their limited size and beam sensitivity, the atomic structure of such particles may become extremely challenging to determine. Therefore keeping the incoming electron dose to a minimum is important. However, this may reduce the reliability of quantitative ADF STEM which will here be demonstrated for nano-particle atom-counting. Based on experimental ADF STEM images of a real industrial catalyst, we discuss the limits for counting the number of atoms in a projected atomic column with single atom sensitivity. We diagnose these limits by combining a thorough statistical method and detailed image simulations.

Keywords: High-resolution scanning transmission electron microscopy (HR

*Corresponding author
Email address: sandra.vanaert@uantwerpen.be (S. Van Aert)
[1] *Phone*: +32 3 2653252
[2] Fax: +32 3 2653318

STEM), Nano-particle atom-counting, Data processing/image processing, Quantitative ADF STEM, Catalyst nano-particles

1. Introduction

The physical and chemical properties of nano-particles are controlled by their exact three-dimensional (3D) morphology, structure and composition. Therefore, characterisation techniques are required to determine the arrangement of all atoms in 3D. Atom-counting using ADF STEM has been shown to be of great efficiency to help characterise the 3D atomic structure when analysing multiple images taken from different crystallographic orientations [1, 2] or even when investigating single images [3, 4]. Atomic resolution ADF STEM images are indeed highly sensitive to the number of atoms [5, 6] and can therefore be used to count the number of atoms in each projected atomic column [7–10]. So far, atom-counting has mainly been demonstrated on model systems which are relatively stable under the incoming electron beam. The purpose of this paper is to elucidate the experimental constraints on the atom-counting reliability which become extremely important when looking at more beam sensitive systems. Therefore, ADF STEM experiments are conducted on a real industrial bimetallic catalyst providing a severe characterisation challenge because of its beam sensitivity and limited size. The inherent limitations of the atom-counting method discussed by De Backer et al. [10] are clearly illustrated by the analysis of the experimental data presented here.

So-called scattering cross-sections, measured from the total intensity of scattered electrons for each atomic column, have been shown to be a very

successful performance measure to count the number of atoms in an atomic column from a single STEM image [7, 9–12]. This measure monotonically increases with the number of atoms in an atomic column in contrast to peak intensities which saturate beyond a certain thickness [13]. Furthermore, scattering cross-sections are robust to many imaging parameters, in particular those that control probe size [13, 14]. These quantities can either be calculated by summing the collected scattering to the ADF detector from probe positions that correspond to a feature [13], or can be obtained by fitting a parametric model of Gaussian peaks to the atomic columns in the experimental image [15]. The volumes under the estimated Gaussian peaks then correspond to the scattering cross-sections [10, 12].

In the literature, two different approaches for atom-counting based on scattering cross-sections are proposed. The first method uses libraries of simulated scattering cross-sections which can be compared to normalised experimental scattering cross-section values [13]. Although this approach is straightforward, it critically depends on accurate knowledge of the experimental detector settings and a-priori structure information. In practice, these parameters require careful measurement or calibration and are not always available, hence limiting the applicability of this method to count the number of atoms. The second method extensively uses statistical techniques to interpret scattering cross-sections [1, 9, 10]. This method can be used without prior knowledge concerning the structure, is independent of image simulations, and provides the percentage of atomic columns for which the number of atoms is identified with single atom sensitivity. However, as discussed by De Backer et al. [10], the reliability of the method depends on

different parameters which can be linked with the quality of the recorded images, such as total number of atomic columns in the experimental STEM image, the number of columns having a different number of atoms, and the amount of noise. In the paper of Van Aert et al. [9], it is shown that only through a combination of the library- and statistics-based method, being completely independent of each other, one is able to count atoms with trustworthy single-atom sensitivity. Here, we will show that this combined method allows us to diagnose limits of atom-counting and to investigate the effect of dose, sampling, background behind the particle of interest, tilt, and sample geometry. The latter parameters become important when studying industrially catalyst particles such as the Pt/Ir mixed alloy nano-particles supported on carbon black discussed in this paper.

The article will be organised as follows. In section 2, the material under study as well as the experimental and simulation details are presented. The methodology to count the number of atoms of a nano-structure is illustrated in section 3. Our findings for atom-counting conducted on catalytic particles are discussed in section 4. Finally, in section 5, conclusions are drawn.

2. Experiment and simulations

Bimetallic nano-particles have shown promise for hydrogen fuel-cell applications; not only do they provide a reduction in the amount of platinum used but they have also demonstrated a significantly higher catalytic activity. Pt/Ir particles in particular show improved resistance to CO poisoning, a by-product in the reforming of hydrocarbons to H_2 gas [16]. The Pt/Ir particles were supported on 3-dimensional carbon black support and received in

powder form dusted onto a carbon coated copper grid. Images were taken at the QuAntEM, a double corrected FEI Titan^3 working at 300 kV with a 20.2 mrad semi-convergence angle under different dose conditions as shown in Fig. 1. The ADF detector ranges from 35 to 190 mrad corresponding to a camera length of 145 mm. For unique atom-counting results, we require a monotonic increase for the scattering cross-sections with thickness.In [17], we show that for small enough particles, such as in this study, a lower ADF detector inner angle is preferred for atom counting because of the higher detected signal for a given incident electron dose. Although coherent contributions are present in the detected signal, a monotonic increase in scattering cross-section is observed for this ADF detector collection range. Furthermore, the scattering cross-sections are robust to tilt when using a lower ADF detector inner angle.

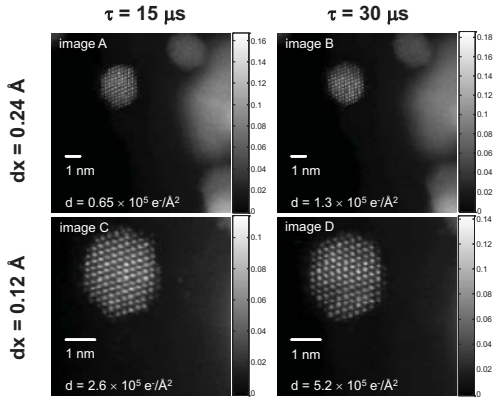

Figure 1: Normalised ADF STEM images of an Pt/Ir particle together with the experimental conditions (dwell time τ, pixel size dx, and incoming electron dose d).

The experimental images were normalised with respect to the incident beam [18, 19] in order to be comparable to image simulations. Image sim-

Parameter	Value
Acceleration voltage	300 kV
Defocus C_1	0 nm
Spherical aberration C_s	406 nm
Convergence angle α	20.2 mrad
Inner detector angle	35 mrad
Outer detector angle	190 mrad
FWHM of the source image	0.7 Å
Debye-Waller factor	0.384 Å^2
Pixel size	0.1154 Å
Zone axis	[110]
Number of phonon configurations	20

Table 1: Parameters for the frozen lattice simulation of Pt.

ulations were performed using the StemSim software [20] under the frozen lattice approach. The simulation settings are listed in Table 1. Since the difference in atomic number only equals 1 for the two elements in the bimetallic nano-particle, the simulated scattering cross-sections of Ir ($Z = 77$) and Pt ($Z = 78$) differ less than 3 % up to 15 atoms in a projected atomic column and therefore for purposes of the analysis presented here they can be treated as being monometallic.

3. Methodology

3.1. Background subtraction

If a spatially-varying background originating from e.g. the carbon support is present in the image, this background has to be subtracted since ignoring it may lead to errors in the quantitative atom-counting results. To account for the image intensity contribution of such a carbon support under the sample, a mask can be generated which contains the region of interest for quantification, i.e. the nano-particle. The intensity outside this mask represents the contribution from the support only and will be used to estimate the values within the mask using a technique known as in-painting. For small areas, and where the support does not contain abrupt changes the simplest form of in-painting, known as iterative Gaussian-blurring or isotropic diffusion, can be used [21].

3.2. Statistics-based atom-counting

In this paragraph, the procedure to count the number of atoms using the statistics-based method [9, 10] is revised and illustrated using image D of Fig. 1. Using statistical parameter estimation theory, the scattering cross-sections can be quantified atomic column-by-atomic column by fitting an empirical imaging model to (background subtracted) experimental images [10, 12, 15]. This empirical imaging model consists of a sum of Gaussian peaks describing the atomic column intensities:

$$f_{kl}(\boldsymbol{\theta}) = \sum_{n=1}^{N} \eta_n \exp\left(\frac{-\left(x_k - \beta_{x_n}\right)^2 - \left(y_l - \beta_{y_n}\right)^2}{2\rho^2}\right) \tag{1}$$

where $\boldsymbol{\theta} = (\beta_{x_1}, \ldots, \beta_{x_N}, \beta_{y_1}, \ldots, \beta_{y_N}, \rho, \eta_1, \ldots, \eta_N,)^T$ are the unknown structure parameters with ρ the width of the Gaussian peak, η_n the height of the

nth Gaussian peak, β_{x_n} and β_{y_n} the x- and y-coordinate of the nth atomic column, respectively, and N the total number of analysed atomic columns. The unknown parameters $\boldsymbol{\theta}$ of the model are estimated in the least square sense. The estimated scattering cross-sections $V_n = 2\pi\eta_n\rho^2$ then correspond to the volumes under the estimated Gaussian peaks. The fitted model for the background subtracted version of image D is shown in Fig. 2(a). The model is in excellent agreement with the experimental data demonstrating its good quality. Next, the estimated scattering cross-sections can be visualised in a histogram in Fig. 2(b). Ideally, this histogram would consist of isolated peaks. However, due to a combination of instabilities of the microscope and sample, and noise effects, the components are smeared out. Therefore, the estimated scattering cross-sections are regarded as a statistical draw from an unknown probability distribution consisting of a superposition of Gaussian components, the so-called Gaussian mixture model:

$$f_{\text{mix}}(V_n; \boldsymbol{\Psi}_G) = \sum_{g=1}^{G} \pi_g \frac{1}{\sqrt{2\pi}\sigma} \exp\left(\frac{-(V_n - \mu_g)^2}{2\sigma^2}\right) \tag{2}$$

This model defines the probability that a specific scattering cross-section value V_n would be estimated for a particular atomic column n. The vector $\boldsymbol{\Psi}_G = (\pi_1, \ldots, \pi_{G-1}, \mu_1, \ldots, \mu_G, \sigma)^T$ contains the unknown parameters π_g, μ_g, and σ being the mixing proportion of the gth component, the mean scattering cross-section of the gth component, and the width of the components, respectively. The parameters $\boldsymbol{\Psi}_G$ can be estimated from the experimental scattering cross-sections using the maximum likelihood estimator for a given number of components G [1, 9, 10, 22]. In practice, the value of G is unknown and has to be inferred from the available scattering cross-sections as

well. The number of significant components, i.e. the model order G, can be retrieved by evaluating the so-called integrated classification likelihood (ICL) criterion, which is shown in Fig. 2(c). This order selection criterion balances the model fit against the model quality. Indeed, the model fit will typically improve for increasing number of components and more details in the available set of scattering cross-sections will be described. However, for high-order models, these details are random and as a consequence the model quality will degrade with the model order. The estimated model order is given by the number of components for which ICL reaches a minimum, which is arrowed in Fig. 2(c). In practice, this minimum often corresponds to a local optimum rather than to a global optimum [10]. Fig. 2(b) shows the estimated Gaussian mixture model. Based on this estimated probability distribution, the number of atoms in a particular projected column can be identified by assigning each scattering cross-section to the component of the mixture model with the largest probability to generate this scattering cross-section. The atom-counts for every column of the nano-particle are shown in Fig. 2(d) .

4. Results and discussions: single atom sensitivity for atom-counting?

In section 3, it is explained and illustrated how measurements for the scattering cross-sections can be obtained atomic column-by-atomic column and how these values can be converted into numbers of atoms. The ultimate goal is to obtain atom-counting results with high precision and high accuracy which are both necessary conditions to conclude single atom sensitivity. High precision can be observed from the Gaussian mixture model when there is nearly no overlap between neighbouring components, such as in Fig. 2(c)

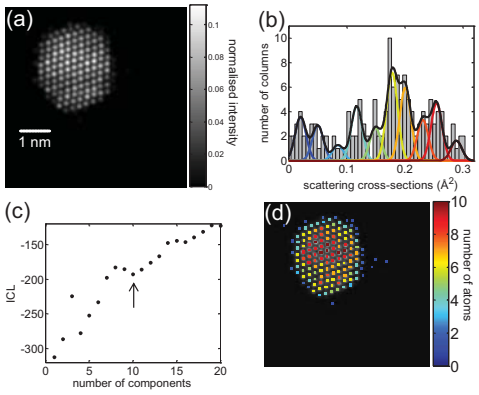

Figure 2: (a) Fitted model of image D (Fig. 1). (b) Histogram of the scattering cross-sections of the atomic columns. The black curve shows the estimated mixture model; the individual components are shown as coloured curves which correspond to the colours for the number of atoms in (d). (c) ICL evaluated as a function of the number of Gaussian components in a mixture model. (d) Number of atoms per column.

for image D. High accuracy can be confirmed when comparing the results of the statistics-based atom-counting method with library values from detailed image simulations. So far, atom-counting has been demonstrated on model systems, which are relatively stable under the incoming electron beam, and this procedure promises single atom sensitivity [9]. In this section, the accuracy of the atom-counting results is investigated for the catalyst of Fig. 1 for which the characterisation is more challenging because of the beam sensitivity and the limited size of the particles. Different parameters which affect the reliability of the atom-counting results are studied.

4.1. Effect of background subtraction

From Fig. 1 it can be seen that a spatially-varying background is present in the images. This background has been subtracted following the method

described in paragraph 3.1. In Fig. 3, the effect of the background subtraction on the atom counts is illustrated. Fig. 3(a) shows the difference map of the atom counts per atomic column with and without background subtraction and Fig. 3(b) shows the vertically averaged mean error in atom counts. Ignoring the spatially-varying background clearly leads to a counting error of ± 1 atom. This type of error thus results from bias of the estimated scattering cross-sections caused by model misspecification [23]. The subtracted background represents the carbon support and is shown in Fig. 3(c). As expected, the reconstructed carbon-ramp corresponds to the mean error in atom counts of Fig. 3(b).

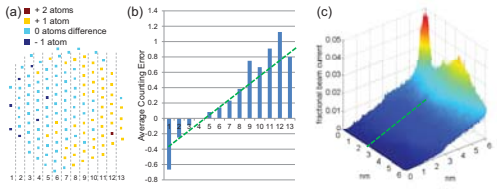

Figure 3: (a) The error observed when the carbon intensity is not considered. (b) Vertically averaged error. (c) The observed carbon contribution in the background-only image.

4.2. Comparison with simulations

In order to check the accuracy, the estimated mean scattering cross-sections of the components are compared with the library values from the detailed image simulations for this experiment. The library values are shown for Pt, the values for Ir are not plotted on this graph since they cannot be distinguished from the scattering cross-sections of Pt up to 15 atoms. From Fig. 4, where the library values are shown for Pt, it can be seen that for image D an excellent match has been found between the estimated mean scatter-

ing cross-sections from the experiment and the simulated values within the expected $5-10$ % error range proving that the number of components when using the ICL criterion as well as the locations of these components in Fig. 2(c) are accurately determined. Slight deviations cannot be avoided because of remaining uncertainties in the microscope settings and practical limitations to fully take the complex dependence of the Debye-Waller factor on both the particle's size and its different behaviour for surface atoms as compared to bulk-like atoms into account [24–26].

Similar analyses were performed for images A, B, and C and their results are also shown in Fig. 4. A mismatch between the estimated and simulated scattering cross-sections can be observed for image C, but is apparent and most pronounced for images A and B. For these images, the number of components in the probability distribution is considerably underestimated. Based on a comparison with the library values, 13 and 15 components are expected for image A and B, respectively. In the following paragraphs, the origin of the mismatch of images A, B, and C with the library values are discussed.

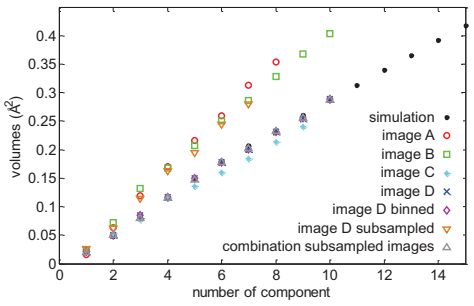

Figure 4: Overview of the analysed data in comparison with the simulations.

4.3. Effect of sample mis-tilt

The slight mismatch of image C from the simulated curve in Fig. 4 stems from a small sample mis-tilt [13]. This can be understood from electron channelling. This phenomenon, where an aligned column of atoms parallel to the incident beam direction exhibits a small lensing effect on the beam, causes a column of atoms to have a larger scattering cross-section than the sum of the individual scattering cross-sections of its constituent atoms [13]. This results in a percentage loss in scattering cross-section for small sample mis-tilts away from a low order zone axis. The mis-tilt measured based on a geometry calculation and the ellipticity of the column equals 31.6 mrad for image C. Based on image simulations, this corresponds to $\sim 7\%$ loss of cross-section which is in agreement with the results shown in Fig. 4. One should be particularly aware of this effect for beam sensitive samples which are liable to reconstruct and rotate under the beam.

4.4. Effect of sampling

The effect of sampling on the atom-counting results is considered since the pixel size of image A and B is double the pixel size (half the magnification) of image D, as can be seen from Fig. 1. Consequently, the number of sampling points in image A and B is half as many with respect to image D. From E et al. [13], it is shown that pixel size has no effect on the scattering cross-sections in the absence of noise. Here, the effect of sampling on the atom-counting analysis is studied by analysing a new image generated by binning 2×2 pixels of image D. In that case, the estimated mean scattering cross-sections are still perfectly in accordance with the simulated values as can be concluded from Fig. 4. This means that sampling itself has no effect

on the accuracy of the atom counts so long as atomic resolution is preserved in the ADF STEM image. The underestimation of the model order for image A and B can thus not be explained as a sampling effect.

4.5. Effect of dose

In the previous paragraph, the effect of sampling was studied as a possible reason for the underestimation of the number of components in images A and B. It should be noticed that while binning 2×2 pixels, the total recorded electron dose is preserved such that only the effect of sampling is studied. However, the electron dose is 4 times lower in image B as compared with image D, and even 8 times lower for image A. This suggests that a reduction of incoming electron dose causes an underestimation of the model order when evaluating the ICL criterion. The lower magnification and electron dose of image B with respect to image D can be mimicked by subsampling image D, i.e. by taking every second pixel in x and y (one quarter overall). The result of the analysis of the subsampled image D is also shown in Fig. 4. This result resembles the analysis of images A and B thus explaining the mismatch with the simulation for these images. The reduced dose leads to less precise measurements of the scattering cross-sections resulting in insufficient statistics for the determination of the number of components by the evaluation of the ICL criterion. The effect of dose on the accuracy of the atom-counting results will be discussed in more detail in the following paragraph.

4.6. Discussion of the accuracy of the atom-counting results

The most pronounced mismatch with the simulations in Fig.4 can be explained as an effect of reduced dose, resulting in less accurate measurements

for the number of atoms in an atomic column. This effect of the reduced dose can be studied in more detail from the Gaussian mixture model. If the dose is reduced, the neighbouring components of the Gaussian mixture model start overlapping more, because of the less precise measurements of the scattering cross-sections. This significant overlap between neighbouring components in the Gaussian mixture model can be measured in terms of the relative width of the components. This relative width expresses the ratio of the width of the components of the Gaussian mixture model and the average increment in scattering cross-section for 1 extra atom, i.e. the σ/δ-ratio. In De Backer et al. [10], it has been shown that this σ/δ-ratio in combination with the N/G-ratio is important when it comes to accurately determining the minimum of the ICL, where N is the number of analysed atomic columns in the ADF STEM image and G the true model order. The probability of choosing the wrong number of components based on the minimum of the ICL is shown in Fig. 5 as a function of the σ/δ-ratio and the N/G-ratio. The corresponding values for image D and subsampled image D are indicated in Fig. 5 to illustrate the effect of the reduced dose. It is clear that the reduced dose widens the components hence limiting the precision. As a consequence the probability for choosing the correct minimum of the ICL significantly decreases. Nevertheless, Fig. 5 suggests that this loss in accuracy can be compensated by increasing the N/G-ratio. In practice, this can be realised by analysing collectively the scattering cross-sections originating from images recorded under the same conditions. From Fig. 5, it can be seen that a combination of 4 images should be sufficient. The results of such a combined analysis of the collective scattering cross-sections originating from

4 different subsampled versions of image D is shown in Fig. 4. The estimated mean scattering cross-sections again coincidence with the library values. It is important to mention that this collective analysis only pays off in terms of accuracy but leaves the precision unaffected. Indeed, the precision of the atom-counting results is determined by the overlap in the Gaussian mixture model and is set by the precision with which the scattering cross-sections are known. This precision is characterised by the electron dose and the value of the scattering cross-section, but is independent of the number of analysed scattering cross-sections. For low dose acquisitions, the precision could in principle be compensated when averaging 'identical' images prior to determine scattering cross-sections. In practice, however, the assumption of multiple images of exactly the same structure is very unrealistic, especially for beam sensitive samples.

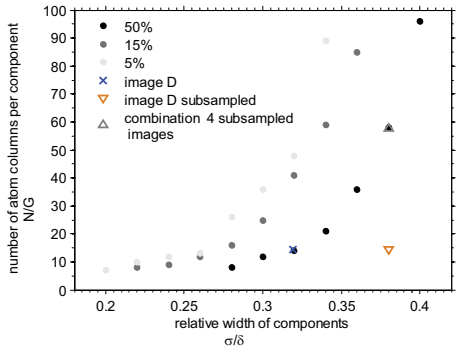

Figure 5: Probability of choosing the wrong number of components based on ICL as a function of σ/δ and N/G. The corresponding values for image D, subsampled image D, and a combination of 4 subsampled images are also shown.

5. Conclusions

In conclusion, it has been shown that the interplay of several effects can greatly impact the reliability of atom-counting in quantitative ADF. This includes parameters such as electron-dose and lateral sampling, but also aspects often beyond the control of the experimentalist, including particle tilt and contrast contributions from the carbon support. Here we report for the first time a study of the minimum dose and sampling requirements to count atoms with single-atom sensitivity using a proposed hybrid statistical and library method to quantify experimental images. We discover that a compensation should be made for the varying sample support to avoid atom-counting errors and that care must be taken in the interpretation of column intensity for slightly tilted nano-particles. For samples that do undergo transformation under the beam, poor image quality cannot be countered by simple image averaging, rather the frames must be analysed collectivity. Finally, our study suggests that while dose is often lowered to reduce sample damage, some minimum level is required to retain single-atom precision. This trade-off between damage and reliability then guides experiment design suggesting that optimum dose and sampling conditions exist for each instrument / sample such that the highest possible precision can be obtained from the hardware available.

6. Acknowledgements

The authors acknowledge financial support from the Research Foundation Flanders (FWO, Belgium) through project fundings (G.0393.11, G.0064.10 and G.0374.13) and a PhD research grant to A. De Backer. The research lead-

ing to these results has received funding from the European Union Seventh Framework Programme under Grant Agreement 312483 - ESTEEM2 (Integrated Infrastructure Initiative-I3), ERC Starting Grant 278510 Vortex, and the UK Engineering and Physical Sciences Research Council (EP/K032518/1). The authors acknowledge Johnson-Matthey for providing the sample and PhD funding to K.E. MacArthur. A. Rosenauer is acknowledged for providing the StemSim program.

7. References

[1] S. Van Aert, K. J. Batenburg, M. D. Rossell, R. Erni, G. Van Tendeloo, Three-dimensional atomic imaging of crystalline nanoparticles, Nature 470 (2011) 374–377.

[2] S. Bals, M. Casavola, M. A. van Huis, S. Van Aert, K. J. Batenburg, G. Van Tendeloo, D. Vanmaekelbergh, Three-Dimensional Atomic Imaging of Colloidal Core-Shell Nanocrystals, Nano Letters 11 (8) (2011) 3420–3424.

[3] S. Bals, S. Van Aert, C. P. Romero, K. Lauwaet, M. J. Van Bael, B. Schoeters, B. Partoens, E. Yücelen, P. Lievens, G. Van Tendeloo, Atomic scale dynamics of ultrasmall germanium clusters., Nature Communications 3 (2012) 897.

[4] P. Kundu, S. Turner, S. Van Aert, N. Ravishankar, G. Van Tendeloo, Atomic Structure of Quantum Gold Nanowires: Quantification of the Lattice Strain, ACS Nano 8 (2014) 599–606.

[5] P. Hartel, D. Rose, C. Dinges, Conditions and reasons for incoherent imaging in STEM, Ultramicroscopy 63 (1996) 63–114.

[6] P. M. Voyles, D. A. Muller, J. L. Grazul, P. H. Citrin, H.-J. L. Gossmann, Atomic-scale imaging of individual dopant atoms and clusters in highly n-type bulk Si, Nature 416 (2002) 826–829.

[7] A. Singhal, J. C. Yang, J. M. Gibson, STEM-based mass spectroscopy of supported Re clusters, Ultramicroscopy 67 (1997) 191–206.

[8] J. M. LeBeau, S. D. Findlay, L. J. Allen, S. Stemmer, Standardless atom counting in scanning transmission electron microscopy, Nanoletters 10 (2010) 4405–4408.

[9] S. Van Aert, A. De Backer, G. T. Martinez, B. Goris, S. Bals, G. Van Tendeloo, A. Rosenauer, Procedure to count atoms with trustworthy single-atom sensitivity, Phys. Rev. B 87 (2013) 064107.

[10] A. De Backer, G. T. Martinez, A. Rosenauer, S. Van Aert, Atom counting in HAADF STEM using a statistical model-based approach: methodology, possibilities, and inherent limitations, Ultramicroscopy 134 (2013) 23–33.

[11] M. Retsky, Observed single atom elastic cross sections in a scanning electron microscope, Optik 41 (1974) 127.

[12] S. Van Aert, J. Verbeeck, R. Erni, S. Bals, M. Luysberg, D. Van Dyck, G. Van Tendeloo, Quantitative atomic resolution mapping using high-angle annular dark field scanning transmission electron microscopy, Ultramicroscopy 109 (2009) 1236–1244.

[13] H. E, K. E. MacArthur, T. J. Pennycook, E. Okunishi, A. J. D'Alfonso, N. R. Lugg, L. J. Allen, P. D. Nellist, Probe integrated scattering cross sections in the analysis of atomic resolution HAADF STEM images, Ultramicroscopy 133 (2013) 109–119.

[14] G. T. Martinez, A. De Backer, A. Rosenauer, J. Verbeeck, S. Van Aert, The effect of probe inaccuracies on the quantitative model-based analysis of high angle annular dark field scanning transmission electron microscopy images, Micron 63 (2014) 57–63.

[15] A. J. den Dekker, J. Gonnissen, A. De Backer, J. Sijbers, S. Van Aert, Estimation of unknown structure parameters from high-resolution (S)TEM images: What are the limits?, Ultramicroscopy 134 (2013) 34–43.

[16] T. R. Ralph, M. P. Hogarth, Catalysis for Low Temperature Fuel Cells Part II: The Anode Challenges, Platinum Metals Review 46 (3) (2002) 117–135.

[17] A. De Backer, A. De wael, J. Gonnissen, S. Van Aert, Optimal experimental design for nano-particle atom-counting from high-resolution STEM images, Ultramicroscopy-doi:http://dx.doi.org/10.1016/j.ultramic.2014.10.015.

[18] J. M. LeBeau, S. Stemmer, Experimental quantification of annular dark-field images in scanning transmission electron microscopy, Ultramicroscopy 108 (2008) 1653–1658.

[19] A. Rosenauer, K. Gries, K. Müller, A. Pretorius, M. Schowalter, A. Avramescu, K. Engl, S. Lutgen, Measurement of specimen thickness and composition in $Al_xGa_{1-x}N/GaN$ using high-angle annular dark field images, Ultramicroscopy 109 (2009) 1171–1182.

[20] A. Rosenauer, M. Schowalter, Stemsim - a new software tool for simulation of STEM HAADF Z-contrast imaging, in: A. Cullis, P. Midgley (Eds.), Microscopy of Semiconducting Materials 2007, Vol. 120 of Springer Proceedings in Physics, Springer Netherlands, 2008, pp. 170–172.

[21] M. M. Oliveira, B. Bowen, R. McKenna, Y.-S. Chang, Fast Digital Image Inpainting, in: Proceedings of the International Conference on Visualization, Imaging and Image Processing (VIIP 2001), Marbella, Spain, 2001.

[22] G. McLachlan, D. Peel, Finite Mixture Models, Wiley series in probability and statistics, John Wiley and Sons, inc., 2000.

[23] A. J. den Dekker, S. Van Aert, A. van den Bos, D. Van Dyck, Maximum likelihood estimation of structure parameters from high resolution electron microscopy images. Part I: A theoretical framework, Ultramicroscopy 104 (2005) 83–106.

[24] B. C. Clark, R. Herman, R. F. Wallis, Theoretical Mean-Square Displacements for Surface Atoms in Face-Centered Cubic Lattices with Applications to Nickel, Physical Review 139 (3A) (1965) A860–867.

[25] P.-A. Buffat, Size effect modifications of the Debye-Waller factor in small gold particles, Solid State Communications 23 (1977) 547–550.

[26] R. Aveyard, R. Ferrando, R. L. Johnston, J. Yuan, Modeling Nanoscale Inhomogeneities for Quantitative HAADF STEM Imaging, Physical Review Letters 113 (075501).